DR VLADIMIR I. POLSHAKOV (Orcid ID : 0000-0002-3216-5737)

Received Date : 09-Dec-2019
Revised Date : 20-Feb-2020
Accepted Date : 30-Mar-2020

Color : Fig 1-10 SuppInfo : 8fig

Williams–Beuren syndrome-related methyltransferase WBSCR27: cofactor binding and cleavage

Sofia S. Mariasina[1†], Chi-Fon Chang[2†], Olga A. Petrova[1], Sergey V. Efimov[3], Vladimir V. Klochkov[3], Olga I. Kechko[4], Vladimir A. Mitkevich[4], Petr V. Sergiev[1,5], Olga A. Dontsova[1,5], and Vladimir I. Polshakov[1*]

[1] M.V. Lomonosov Moscow State University, Moscow 119991, Russia

[2] Genomics Research Center, Academia Sinica, Taipei, Taiwan

[3] NMR Laboratory, Institute of Physics, Kazan Federal University, Kazan 420008, Russia.

[4] Engelhardt Institute of Molecular Biology, Russian Academy of Sciences, 32 Vavilova str., Moscow, 119991, Russia

[5] Skolkovo Institute of Science and Technology, Moscow, Russia

[†] The authors wish it to be known that, in their opinion, the first two authors should be regarded as joint First Authors.

* To whom correspondence should be addressed. Tel: +7 916 1653928, Email: vpolsha@fbm.msu.ru.

***Running title*: Interaction of methyltransferase WBSCR27 with cofactor**

***Keywords*:** SAM-dependent methyltransferases, Williams-Beuren syndrome, Protein NMR, SAH hydrolysis, NMR resonance assignment

***Abbreviations*:** ACP, 3-amino-3-carboxypropyl; 5'dAdo, 5'-Deoxyadenosine; Ade, Adenine; HSQC, Heteronuclear Single Quantum Coherence Spectroscopy; MTase, methyltransferase; MTA, 5'-Deoxy-5'-methylthioadenosine; SAH, S-(5'-adenosyl)-L-homocysteine; SAM, S-(5'-adenosyl)-L-methionine; WBSCR27, Williams-Beuren Syndrome Chromosome Region 27 protein.

ABSTRACT

Williams-Beuren syndrome, characterized by numerous physiological and mental problems, is caused by the heterozygous deletion of chromosome region 7q11.23, which results in the disappearance of 26 protein coding genes. Protein WBSCR27 is a product of one of these genes whose biological function has not yet been established and for which structural information has been absent until now.

Using NMR, we investigated the structural and functional properties of murine WBSCR27. For protein in the apo form and in a complex with S-(5'-adenosyl)-L-homocysteine (SAH), a complete NMR resonance assignment has been obtained and the secondary structure has been determined. This information allows us to attribute WBSCR27 to Class I methyltransferases. The interaction of WBSCR27 with the cofactor S-(5'-adenosyl)-L-methionine (SAM) and its metabolic products – SAH, MTA and 5'dAdo – was studied by NMR and isothermal titration calorimetry. SAH binds WBSCR27 much tighter than SAM, leaving open the question of cofactor turnover in the methylation reaction. One possible answer to this question is the presence of weak but detectable nucleosidase activity for WBSCR27. We found that the enzyme catalyzes the cleavage of the adenine moiety from SAH, MTA, and 5'dAdo, similar to the action of bacterial SAH/MTA nucleosidases. We also found that the binding of SAM or SAH causes a significant change in the structure of WBSCR27 and in the conformational mobility of the protein fragments, which can be attributed to the substrate recognition site. This indicates that the binding of the cofactor modulates the folding of the substrate-recognizing region of the enzyme.

INTRODUCTION

Protein WBSCR27 is a product of the gene of the same name in the chromosome region 7q11.23. Heterozygous deletion of this region is associated with a rare but severe genetic disease – Williams–Beuren syndrome (WBS), characterized by numerous physiological and mental problems [1]. Patients with WBS have abnormalities in the cardiovascular, endocrine, and nervous systems that affect morbidity and mortality [2]. Deletion of the Williams–Beuren Syndrome Chromosome Region (WBSCR) in 98% of patients leads to disappearance of ~1.5 million DNA base pairs encompassing 26 coding genes [3]. Many, though not all, expression products of these genes are annotated and their intracellular functions are established [2, 3]. One such identified protein is S-adenosyl-L-methionine (SAM)-dependent rRNA methyltransferase (MTase), encoded by the WBSCR22 gene [4, 5]. The WBSCR22 protein (also known as Bud23) is required for pre-ribosomal RNA processing and mediates N^7 methylation of G1639 in human 18S rRNA [6, 7]. Protein WBSCR27 shows a high level of homology to WBSCR22 (E-value = 3×10^{-9}) and bioinformatics analysis of the sequence of WBSCR27 indicates that this protein also belongs to the family of Class I SAM-dependent MTases [8]. However, in contrast to WBSCR22, the exact biological function of WBSCR27 remains unclear and the substrate of the methylation reaction catalysed by this MTase is still unknown.

There are five main classes (I–V) of MTases, each with structurally distinct folding [9]. The largest is Class I proteins which have the canonical Rossmann fold comprising a β-sheet flanked by two layers of α-helices to form an αβα sandwich. The β-sheet consists of seven β strands (β_1–β_7) which alternate with six α-helices, three helices located on each side of the sheet [10]. The structural core of the Rossmann fold is mainly responsible for SAM binding, while substrate recognition is usually maintained by the auxiliary domains or additional α-helices [9]. There are two conserved motifs common to all Class I MTases: a GxG fragment located between β_1 and helix α_A, and an acidic residue located in a strongly conserved position at the end of the β_2 strand, which forms hydrogen bonds with two hydroxyl groups of the SAM ribose [11]. Other residues participating in SAM binding vary from one subgroup of Class I MTases to another, ensuring the proper orientation of the reactive methyl group of the SAM molecule towards its target acceptor [12]. This property, together with the presence of additional substrate recognition domains, determines the extremely high substrate specificity of the enzyme, providing a unique biological function for each MTase.

A large range of substances can be substrates of the Class I MTases, ranging from small molecules to DNA, RNA, and proteins. Small molecule methylation is part of the biosynthesis and modification of bioactive molecules including membrane components, protein cofactors, prosthetic groups, pigments, and signalling and defence compounds [13]. Methylation of DNA affects chromatin compaction and plays a key role in the regulation of gene expression, embryonic development, genomic imprinting, and carcinogenesis in eukaryotic cells [14], as well as defence against bacteriophages, mismatch repair, and control of DNA replication timing in prokaryotic cells [15]. RNA methylation regulates the translation, stability, and transport of mRNA, quality control of ribonucleoprotein assembly, resistance to antibiotics, deciphering of normal and altered genetic code, splicing regulation, immune response, and other functions [16, 17]. Protein methylation is involved in the regulation of almost every aspect of cell biology through its alteration of the functional properties of proteins [18].

SAM is a cofactor for almost all known MTases [19], acting as a CH_3-group donor in methylation reactions. SAM is the second most common intracellular cofactor after ATP [20]. At neutral and alkaline pH, SAM undergoes spontaneous degradation in two parallel directions: cleavage to methylthioadenosine (MTA) and homoserine lactone, and hydrolysis to adenine and S-ribosyl-L-methionine [21]. The presence of the trivalent sulfur atom determines the main pathways of SAM metabolism in cells [22, 23] (Scheme 1), including (i) removal of the methyl group in a methylation reaction with formation of S-(5'-adenosyl)-L-homocysteine (SAH), (ii) cleavage of the bond between the sulfur and carbon of the methionine chain with formation of MTA and homoserine lactone, and (iii) radical SAM (RS) enzyme-catalysed cleavage of the bonds between the sulfur and neighbour carbons with the formation of the following reactive radicals: 5'-deoxyadenosyl radical [24], 3-amino-3-carboxypropyl (ACP) radical [25], or methyl radical [26].

For most MTases, SAH is a competitive inhibitor with binding affinity comparable to, or often higher than, that of SAM [27]. Therefore, cell homeostasis of SAM and SAH must be very precisely regulated, particularly by SAH degradation after methylation. In eukaryotes, SAH is broken up to form adenosine and homocysteine in the reaction catalysed by SAH hydrolase [27]. In contrast, in prokaryotic cells, the predominant route of SAH metabolism is the formation of adenine and S-ribosylhomocysteine catalysed by SAH nucleosidase [28]. All known prokaryotic nucleosidases are three-substrate enzymes capable of cleaving adenine not only from SAH but also from MTA and 5'dAdo [29].

In our work, we studied murine WBSCR27 using the methods of NMR spectroscopy and isothermal calorimetry. Earlier, we determined assignments of the NMR signals of WBSCR27 in the presence of SAM and characterized the protein's secondary structure and backbone dynamics [8]. In this paper, we report the results of NMR studies of WBSCR27 in the apo form and the details of its interactions with SAM, SAH, and related compounds. It was found that the binding of cofactor SAM or co-product SAH induces intensive rearrangement of protein folding. We demonstrated that WBSCR27 participates in the cleavage of both SAM and SAH. These results contribute to understanding of the properties and function of WBSCR27 and its role in WBS.

RESULTS

WBSCR27 is co-purified with both SAM and SAH

To determine the structure and properties of the WBSCR27 protein, we cloned WBSCR27 cDNA in the pET30aTEV vector and expressed it in *E. coli* BL21 (DE3) strain. We found that ^{15}N–^{1}H HSQC spectra of the purified recombinant protein are not reproducible from sample to sample and contain many more resonances than can be expected for the 240 a.a. protein. However, the addition of an excess of either SAM or SAH led to the simplification of the spectrum and disappearance of duplicated signals. The presence of 10 mM SAM in 0.4–0.6 mM WBSCR27 solution led to the formation of stable samples suitable for NMR studies. These samples were used for making the signal assignments for the WBSCR27–SAM complex reported earlier [8]. The results described indicate that the protein obtained after purification exists in a mixture of the apo form and complexes of WBSCR27 with cofactor(s). It should be noted that cofactor(s) is(are) bound very tightly and cannot be removed by dialysis even after 3 days at 5 °C.

To ensure that WBSCR27 was co-purified with the cofactor(s), the protein was denatured by addition of DCl, and the ligands released were identified in the supernatant by ^{1}H NMR (Fig. 1). The ratio of free SAM and SAH was found to be 1:2.7, indicating an excess of the complex of WBSCR27 with SAH after purification. Uniquely identified CH-1' signals of bound ^{13}C-labeled SAM or SAH (6.1 and 86.9 ppm for ^{1}H and ^{13}C correspondingly) could also be observed in the ^{13}C-^{1}H HSQC spectra of protein expressed in ^{13}C-enriched media.

Refolding of WBSCR27 and preparation of apo-WBSCR27

In order to obtain a single-component protein sample, the ability of WBSCR27 to refold was investigated. Heteronuclear NMR spectroscopy was used to test the formation of the native three-dimensional structure of the protein. It was found that dialysis of the protein dissolved in 8 M urea against a buffer solution (details in Materials and Methods) restores the native conformation of WBSCR27. The ^{15}N–^{1}H HSQC spectra of the protein before and after refolding were identical. Preparation of the apo form of the protein required an additional stage of dialysis against 8 M urea for removal of the cofactor(s). The speed of protein refolding is higher than the diffusion rate of both SAM and SAH through the dialysis membrane; therefore, without this additional stage, the protein refolded in the form of complexes with cofactors. The approach described allowed us to obtain apo-WBSCR27 in amounts sufficient for subsequent NMR studies.

NMR chemical shift assignment for apo-WBSCR27

Chemical shift assignment for WBSCR27 in its apo form was performed using ^{13}C–^{15}N-labelled samples obtained by the method described above. Backbone amide ^{1}H and ^{15}N resonance assignment (Fig. 2) was achieved for 193 of 224 non-proline residues (86%). Amide signals could not be identified for residues 18–23, 31–35, 45, 49–50, 54–55, 141, 143, 145–146, 148, 151, 171, 175–177, 207, 228, and 231, for which the signals were missing in ^{15}N–^{1}H HSQC due to conformational exchange and/or fast exchange of amide protons with water and subsequent broadening of the signals. The overall completeness of the backbone chemical shift assignment was 78%, with 90% for Cα, 85% for C', 82% for Cβ, and 39% for Hα resonances. Side-chain assignments were obtained from the analysis of the 3D ^{13}C HCCH-TOCSY experiment.The chemical shift assignments of the apo form of WBSCR27 have been deposited in the BioMagResBank (http://www.bmrb.wisc.edu) under accession number **BMRB-27578**.

Values of the $^{1}H\alpha$, $^{13}C\alpha$, $^{13}C\beta$, $^{13}C'$, and ^{15}N chemical shifts were used to determine the secondary structure of the apo form of WBSCR27 and identify flexible regions of the protein backbone using TALOS+ [30]. The core of the apo-protein (α/β/α 'sandwich') is identical to that determined in the complex of WBSCR27 with SAM [8]. It contains seven β-strands alternated with six α-helices. However, in contrast to the complex with the cofactor, where the N-terminal region is ordered and contains three α-helices, the apo form of WBSCR27 has a long unstructured N-terminal tail (Fig. 3). Two α-helices (α1 and α2), well formed in the complex, are absent in the apo form, and helices α3 and α4 are much shorter.

Stability of binary complexes of WBSCR27 with SAM and SAH

The apo form of WBSCR27 was used for the preparation of complexes of the protein with either SAM or SAH. ^{15}N–^{1}H HSQC spectra recorded for the complex of WBSCR27 with SAH, without an excess of the ligand, indicated that at 35 °C the complex slowly undergoes transformation to the apo form (Fig. 4). It takes ~17 days for ~90% conversion. Such transformation is associated with ligand decomposition rather than with its dissociation. Thus, several new sharp peaks of low-molecular weight compounds appeared in the ^{1}H NMR spectrum. Some of the peaks belong to adenine: the addition of small amounts of free adenine to the reaction mixture led to an increase in the intensity of these signals but not to the appearance of additional resonances. The results described indicate that SAH undergoes cleavage of the adenine fragment from the ribose moiety. This reaction occurs only in the presence of WBSCR27. Without the protein, SAH remains stable for more than 70 days in the same conditions (Fig. S1).

SAM bound to WBSCR27 undergoes transformation to SAH, which was monitored in the series of ^{15}N–^{1}H HSQC spectra (Fig. 5). This transformation was much faster than the cleavage of adenine: after 3 h at 35 °C, more than 40% of SAM turned into SAH, which allowed us to estimate a half-life for conversion of the cofactor within the protein in the range from 4 to 5 h. Free SAM underwent much slower transformation to MTA plus homoserine lactone, and S-ribosyl-L-methionine plus adenine (Fig. 6 A,B). The presence of catalytic amounts of WBSCR27 did not noticeably accelerate the speed of SAM degradation (Fig. 6 C,D).

Nucleosidase activity of WBSCR27

It is known that the enzymes capable of excising adenine from SAH can also catalyse the cleavage of adenine from MTA and 5'dAdo. Adenine excision from these three substrates catalysed by WBSCR27 was studied by NMR. Accumulation of adenine and a decrease in the amounts of SAH, MTA, and 5'dAdo was observed in the ^{1}H NMR spectra of incubation mixtures after addition of WBSCR27 (Fig. 7). WBSCR27 catalysed adenine excision from all three substrates (Scheme 2). In all cases, the rate of the nucleosidase reaction was slow (i.e. the rate constant was less than 8×10^{-7} s^{-1} for 5'dAdo) and Michaelis constants could not be reliably determined from the time curves of the NMR intensity changes. A similar experiment was performed with adenosine; however, it was found that WBSCR27 does not cleave it.

It should be noted that adenine removal leads to the formation of products that bind to the protein much more weakly than SAH, which allows them to be separated from the protein by dialysis. This is another way to obtain the apo form of the protein (though less effective). The ^{15}N–^{1}H HSQC spectra of the apo-WBSCR27 obtained by this approach were identical to the spectra of the refolded protein, which confirms the correctness of the refolding process.

WBSCR27 interaction with SAM, SAH, MTA, 5'dAdo, and adenine

Heteronuclear NMR spectroscopy and isothermal titration calorimetry (ITC) were used to study interactions of SAM, SAH, MTA, 5'dAdo, and adenine with WBSCR27. For NMR experiments, the ^{15}N-enriched apo form of WBSCR27 was titrated with an increasing amount of the studied ligands. We found that the binding of SAM and SAH occurs in a slow exchange limit (in the NMR time scale): there are two sets of signals in the NMR spectra, which belong to both the apo form of the protein and the corresponding complex. The binding of MTA, 5'dAdo, and adenine to WBSCR27 is much weaker than the binding of SAH or SAM. In the case of these three ligands, NMR spectra corresponded to fast exchange between free and bound states. Therefore, protein resonances moved upon an increase of the ligand portion, from their positions characteristic of the apo form to positions characteristic of the corresponding complexes. Estimated values of K_d were 40 ± 10 μM for MTA and 100 ± 60 μM for 5'dAdo at 35 °C.

ITC was used to obtain more precise thermodynamic characteristics of the interactions of WBSCR27 with SAM and SAH (Fig. S2). Stoichiometry of the binding for both ligands was 1: 1. The binding of SAM and SAH to WBSCR27 was studied at three different temperatures, 15, 25, and 37 °C, and the results are summarized in Tables 1 and 2. The affinity of WBSCR27 for SAM decreased eight-fold when the temperature increased from 15 °C (K_d = 0.4 μM) to 37 °C (K_d = 2.9 μM). The K_d value for SAH binding to WBSCR27 increased 20-fold from 0.08 μM (15 °C) to 1.61 μM (37 °C).

Plotting the enthalpy of interaction versus temperature, we obtained heat capacity change (ΔC_p) values for WBSCR27 interactions with SAM and SAH (Table 2). The binding of WBSCR27 was characterized by an immense ΔC_p of −530 and −660 cal mol^{-1} K^{-1} for SAM and SAH, respectively.

Changes in the heat capacity are believed to reflect the change in the solvent-accessible area (SAA) during the process [31]; a wealth of available experimental data has been analysed,

providing an empirical formula connecting the change in ΔC_p and the change in the solvent-accessible area: $\Delta C_p = 0.27\Delta A_{aromatic} + 0.4\Delta A_{non\text{-}aromatic}$, where $\Delta A_{aromatic}$ and $\Delta A_{non\text{-}aromatic}$ are the protected areas due to aromatic and non-aromatic amino acids in $Å^2$, respectively [32]. This formula was used to translate the ΔC_p values into SAA change estimates (Table 2).

It is interesting to note that SAH, a co-product of the methylation reaction, binds to the protein with a higher affinity than the cofactor, SAM.

Mapping the binding sites of SAM, SAH, and their fragments

Assignment of the chemical shifts in NMR spectra of apo-WBSCR27 and protein complexes with SAM and SAH, as well as assignment of the ^{15}N and ^{1}H signals of protein backbone amide groups obtained upon titration of the protein apo form by MTA, 5'dAdo, and adenine (Figs S3–S5), allowed mapping of the binding site of the ligands. Fig. 5 shows the ^{15}N and ^{1}H chemical shift perturbation caused by ligand binding. It should be noted that the magnitude of the ligand-induced chemical shift changes generally increased in the series Ade > 5'dAdo > MTA > SAH (Fig. S6). However, for some amino acid residues, for example, G123 (Fig. S6A), V83 (Fig. S6B), and V140 (Fig. S6C), deviation in the direction of the chemical shift was observed. ^{1}H and/or ^{15}N resonances of the amide groups of these residues shifted with an increasing concentration of MTA, 5'dAdo, and Ade in one direction, and upon binding to SAH, in the opposite direction.

Residues having large chemical shift changes between apo-WBSCR27 and its complex with SAH are highlighted in the model of the WBSCR27 protein (Fig. 8). In general, the greatest changes in chemical shifts were observed upon interaction of the protein with SAH (Fig. 8A) and SAM (Fig. 8B). Changes in chemical shifts of the residues located in loops between β2 and α6 (β2/α6), β3/β4, and at the edge of strand β4 were of comparable magnitude for all studied ligands except adenine. This indicates that the binding site of the nucleoside moiety is located in this region. The methionine fragment of the cofactor is located near the loop β1/α5 and helices α3 and α4. Binding of both SAM and SAH, but not their smaller fragments, also stimulated the formation of helices α1–α3. In apo-WBSCR27, this whole region is unstructured and flexible (Fig. 3). SAH and SAM induced chemical shift changes of similar sign and magnitude; however, there were some differences between these two complexes (Figs. 5 and 8A,B). The protein regions with the largest differences in chemical shifts between complexes with SAH and SAM were the loops

β1/α5, β6/β7, and α3/α4. The largest chemical shift differences were observed for residues A52, G79, G81, V83, G100, S101, L117, C120, V140, T170, and G229.

DISCUSSION

WBSCR27 adopts the canonical Rossmann fold

Assignment of the chemical shifts of WBSCR27 in both the apo state and in complex with the cofactor, and related information on the protein secondary structure, makes it possible to unambiguously attribute the WBSCR27 protein to the Class I MTases with a canonical Rossmann fold. Multiple sequence alignment of the WBSCR27 protein and several Class I MTases with a determined three-dimensional structure (Fig. S7) shows the high level of structural similarity of the β-sheet protein core, despite the low level of their sequence identity. Seven β-strands with the topology $\beta_6\uparrow\beta_7\downarrow\beta\uparrow_5\uparrow\beta_4\uparrow\beta_1\uparrow\beta_2\uparrow\beta_3\uparrow$ retain their spatial arrangement in all the structures examined (Fig. 9). At the same time, among the helices, only α5 and α7 retain their length and location. All other α-helices vary in their length and relative position. In some cases, one or two helices can be absent (as in the case of WBSCR27 and several other MTases having a loop instead of a helix between strands β3 and β4) or replaced by more complex structural elements, including several helices (Fig. 9 A,C,D) [33-35] or β-sheet fragments (Fig. 9 B,F) [35, 36]. Substrate recognition domains are frequently found at the N-terminal part of MTases [37]. For thiopurine methyltransferase from *Pseudomonas syringae*, metabolizing 6-thiopurine medications, the authors of one study specifically noted the role of its N-terminal fragment in binding of the substrate [35]. The bacterial 16S rRNA MTase RsmD [38] possesses an additional N-terminal β-hairpin [39], while the RlmF 23S rRNA MTase contains an N-terminal extension predicted to contain a small α/β domain [40]. Later, the eukaryotic homologue of RlmF, METTL16, was shown to have this structured extension [41]. A larger N-terminal RNA binding domain is documented for the bacterial RsmB small subunit rRNA MTase [42] and the RsmC small subunit rRNA MTase [43].

In some MTases, the C-terminal substrate recognition domain might be revealed. This is observed, for example, for the *Bacillus subtilis* MTase TrmK, responsible for the N1-methylation of adenosine A22 in tRNA [44], where three C-terminal α-helices are involved in recognition of the methylation substrate (tRNA). C-terminal arrangement of the substrate recognition domain is documented for RsmF 16S rRNA MTase [45], ErmC erythromycin resistance 23S rRNA MTase [46] and many others (see, e.g. [47]).

Obviously, the structure of the β-sheet core is maintained to ensure the optimal position of the bound cofactor relative to the methylation substrate, whereas variable fragments in many cases represent the elements necessary for recognition of the substrate. In the case of WBSCR27, such variable fragments are N-terminal helices α1–α3 and several loops located on the apex of the β-sheet (Figs. 3, 10), including loops 67, β4/α7, and β5/α8. It is logical to assume that such variable regions can form a substrate binding site in WBSCR27.

Position of the cofactor in the complex with WBSCR27

The cofactor binds to MTases in a rather conservative pocket, located at the apex of strands β1, β2, and β4 (Fig. 9 A,B,D,E). It is not surprising that these fragments are the most conserved in the primary structure of the Class I MTases (Fig. S7). Experimental NMR data confirm the position of the cofactor binding pocket in the case of WBSCR27. Thus, the chemical shifts of the amide signals of all the above-listed residues undergo significant changes upon the transition from the apo form of the protein to its complex with its cofactor (Fig. 10). Most of these signals also change their position when the ligand changes from SAM to SAH.

Binding affinity of SAM and SAH

WBSCR27 binds both SAM and SAH so tightly that the protein can only be purified in the bound form. It is known that many MTases are co-purified with the cofactor SAM or co-product SAH. For example, the DENV-3 MTase (Dengue virus serotype 3 MTase) and VNL MTase (West Nile virus MTase) produced in *E. coli* are isolated and purified with SAM [48, 49]. In contrast, the MTase MraW from *Thermotoga maritima* [50] and the protein repair MTase from the hyperthermophilic archaeon *Pyrococcus furiosus* [51] are co-purified with SAH. In most cases, the apo form of the MTase can be obtained only by denaturation of the protein with subsequent refolding [48]. We used an NMR-based method to identify the presence of both ligands (SAM and SAH) in the purified protein. It was found that WBSCR27 isolated from *E. coli* lysate exists as a mixture of complexes with both ligands, and the amount of SAH is almost three times that of SAM.

SAH is a strong competitive inhibitor of all SAM-dependent MTases [52]. SAM binds tighter than SAH in the case of many studied MTases. For instance, the MTase RsmD binds SAM four times tighter than SAH (K_d for SAM and SAH at 25 °C are 0.58 and 2.5 μM, respectively) [53].

However, in our case, WBSCR27 binds SAH more strongly than SAM. A similar example is the dimethyltransferase RosA, which catalyses the final stage of biosynthesis of the antibiotic roseoflavin in *Streptomyces davawensis* [54]. SAH binds to RosA approximately ten times tighter than SAM. It is interesting to note that, at low temperatures, SAH has a five-fold higher affinity for WBSCR27 than SAM. However, at physiological temperature, the binding constant of both ligands has only a two-fold difference.

A greater binding affinity for SAH may be one of the reasons that WBSCR27 is purified primarily in the form of a complex with the co-product, despite the fact that the intracellular concentration of SAM is one to two orders of magnitude higher than the concentration of SAH (in *E. coli*, concentrations of SAM and SAH are 400 μM and 1.3 mM, respectively [55], and in mammalian cells the concentration of SAM also exceeds that of SAH by 5–10 times [56]). The second reason for the smaller amount of bound SAM can be linked to its rather rapid (several hours at 35 °C) conversion to SAH catalysed by WBSCR27 even in the absence of methylation substrates. It is worth noting that the conversion of SAM to SAH within the complex with WBSCR27 proceeds much faster than degradation of the free cofactor. Thus, the half-life of this reaction for the complex of SAM with WBSCR27 is 4–5 h, whereas in the free state it is ~64 h under similar conditions ([21] and Fig. 6). It is very unlikely that WBSCR27 represents the unique example of such quick SAM degradation. Thus, although SAM was used in co-crystallization experiments for obtaining crystals of the complex of *Myxococcus xanthus* catechol-O-methyltransferase, mainly SAH was detected in the crystals [57].

The higher binding affinity of SAH for WBSCR27 compared to SAM raises the question of the mechanism of cofactor turnover after completion of the methylation reaction. It can be assumed that one of the possible mechanisms is the negative cooperative binding effect between the methylation product and the co-product SAH. In this case, the binding affinity of SAH should decrease after methylation of the substrate. However, in the case of the MTase RosA, the binding affinity of SAH in the presence of synthesized roseoflavin, on the contrary, increases [54]. This keeps the cofactor turnover process not fully understood. An alternative mechanism of cofactor turnover can be associated with its catalytic cleavage, for example, as in the case of WBSCR27, via cleavage of the adenine moiety from SAH followed by dissociation of the resulting degradation products.

Nucleosidase activity of WBSCR27

We discovered nucleosidase activity of WBSCR27, featured in excision of the adenine residue from SAH and its analogues (Scheme 2). The rate of this reaction is low, but in the absence of the enzyme it does not occur. It is interesting to note that the rate of adenine cleavage increases in the series SAH, MTA, and 5'dAdo. At the same time, the excision of adenine from adenosine does not occur, although this compound differs from 5'dAdo only by the presence of a single hydroxyl group at position 5'. This fact further confirms the enzymatic nature of this reaction.

Hydrolytic removal of the adenine base from SAH is catalysed by the bacterial enzymes MTA/SAH nucleosidases [58]. These enzymes are involved in the catabolism of SAH and MTA and the regulation of intracellular methylation. However, the pathways of SAH catabolism in eukaryotes and prokaryotes are significantly different, and higher organisms lack annotated enzymes capable of hydrolysing SAH to adenine and ribosylhomocysteine. In eukaryotes, SAH is degraded to adenosine and homocysteine by SAH hydrolase [59]. This difference between prokaryotes and eukaryotes allows the use of MTA/SAH hydrolase as a promising target for rational drug design [60]. All prokaryotic SAH nucleosidases are three-substrate enzymes, catalysing adenine excision not only from SAH but also from two other products of the SAM cycle – MTA and 5'dAdo. WBSCR27 is also able to cleave all three substrates, but its nucleosidase activity is significantly lower compared to bacterial MTA/SAH nucleosidases. However, for this type of catalytic activity, we were not able to find analogues for WBSCR27 among eukaryotic enzymes.

Cofactor binding causes changes in the secondary structure of WBSCR27

One of the most interesting experimental observations resulting from the NMR study of WBSCR27 is the significant changes in the protein's secondary structure and backbone mobility upon cofactor or co-product binding (Figs 3 and 10). Transition from the apo form to the complex results in the formation of three additional N-terminal α-helices (α1–α3). Structuring of this part of the protein is accompanied by a substantial decrease in the mobility of the N-terminal fragment, as well as a decrease in the mobility of loop β4/α7 and the C-terminal fragment of loop 67 (Fig. 3). It is worth noting that all these fragments of WBSCR27 belong to the potential substrate recognition site. Thus, cofactor binding to protein apparently induces the formation of a substrate-recognizing site of WBSCR27.

Our thermodynamic investigations of the interactions of WBSCR27 with SAM and SAH are also indicative of structural rearrangements upon formation of the complexes. One of the parameters of the interactions we measured is a change in heat capacity, ΔC_p, which is believed to reflect the degree of structural rearrangement [31]. In the case of SAM binding to WBSCR27, ΔC_p is significant (−530 cal mol^{-1} K^{-1}, Table 2), suggesting major structural rearrangements with estimated changes in SAA ranging from 1325 to 1963 Å. The binding of SAH causes even greater structural rearrangements of the protein molecule (ΔC_p = −660 cal mol^{-1} K^{-1}, SAA ranging from 1650 to 2444 Å, Table 2).

In this regard, it is interesting to analyse the available examples of changes in Class I MTase conformation during the transition from its apo form to complexes with a cofactor and/or substrate of the MTase reaction. Differences in the orientation of loops β2/α5 and α2/α3 for the apo form and the complex with the cofactor are observed for bacterial (*M. xanthus*) catechol-O-methyltransferase [57]. There are differences in the orientation of loops β6/β7 (loop 67) and α2/α3 in rat catechol-O-methyltransferase for its apo form and the complex with SAM [61]. The orientation of loop 67 is also changed upon binding the inhibitor (3,5-dinitrocatechol, substrate analogue) and formation of the ternary complex [61]. However, all three helices at the N-terminus are present not only in holo form or ternary complex but also in the apo form. For rat liver glycine N-methyltransferase (GNMT), only localized changes of the residues directly involved in the binding of the cofactor or substrate pockets are observed [62]. In the structure of MnmC2, the MTase domain of the bifunctional enzyme responsible for the post-translational modification (methylaminomethylation) of uridine U34 at the wobble position of $tRNA^{Glu}$, $tRNA^{Lys}$, and $tRNA^{Arg}$, there is an unstructured loop near the SAM binding site, which remains unstructured upon binding of the cofactor [63]. Interaction of the *B. subtilis* MTase TrmK, responsible for the formation of m1A22 in tRNA with cofactor and substrate (tRNA), has been studied using NMR [44]. The authors observed a change in the ^{1}H and ^{15}N resonances of the amide groups upon titration of SAH and tRNA to protein; however, these changes were much smaller than those we observed for WBSCR27. Thus, to the best of our knowledge, there is no other example of such large-scale structural changes in the Class I MTases caused by cofactor binding as is found for WBSCR27.

Concluding remarks on the possible substrate of WBSCR27

Despite intensive attempts to determine the exact biological function of WBSCR27, including comparative proteomic experiments using transgenic mice with a knockout of the *Wbscr27* gene, the substrate of this MTase is still unknown. In studies of DNA methylation using zebrafish embryo models, the authors of [64] suggested that the *Wbscr27* gene product is involved in DNA methylation. However, the authors have provided no reliable evidence for this hypothesis. We are inclined to believe that the most likely substrate of the enzyme is not DNA but RNA. This, in particular, is indicated by a certain similarity of WBSCR27 with the RNA MTase WBSCR22 (Bud23). The substrate recognition centre of WBSCR27 is composed of at least three N-terminal α-helices and the large loop 67 (Fig. 10). These fragments contain a sufficient number of residues capable of providing reliable recognition of large biomolecules. We hope that the results obtained in this work will help in determining the methylation substrate and exact biochemical function of this enzyme.

CONCLUSIONS

In the present work, we studied the WBSCR27 protein encoded by one of the genes of unknown function associated with WBS. The secondary structure of the protein determined by NMR allows us to unambiguously assign WBSCR27 to the Class I MTases. Ligand-induced changes of the chemical shifts highlight the binding site of the coenzyme SAM and co-product SAH. We demonstrated that the binding of SAH is tighter than that of the cofactor SAM. It is shown that WBSCR27 binds not only SAM and SAH, but also structurally similar products of SAM metabolism – MTA, 5'dAdo, and adenine. We also found that binding of SAM or SAH causes significant structural rearrangements of the protein. It can be assumed that binding of the cofactor modulates folding of the substrate-recognizing region of the enzyme, thereby preparing it for subsequent binding to the substrate. In addition to the main type of MTase activity of WBSCR27, the enzyme also exhibits weak but detectable nucleosidase activity, catalysing the removal of the adenine moiety from SAH, MTA, and 5'dAdo, which makes it related to bacterial SAH/MTA nucleosidases. This type of enzymatic activity may play a role in the mechanism of cofactor turnover.

MATERIALS AND METHODS

Protein expression and purification

WBSCR27 was expressed in *E. coli* BL21 (DE3) using a pET30aTEV vector containing a 6His-tag, an S-tag, and a TEV cleavage site at the N-terminus of the cloned protein. Cells were transformed with the pET30aTEV-WBSCR27 vector and cultivated in LB medium containing kanamycin (50 μg mL^{-1}) at 37 °C until an optical density of 0.3–0.5 (OD_{600}) was achieved. Then expression was induced with IPTG (isopropyl-thio-β-D-galactoside, 1 mM) and allowed to continue for 14–16 h at 21 °C. Uniform ^{15}N isotope-labelled and ^{13}C and ^{15}N isotope-labelled WBSCR27 were grown and expressed in an M9 minimal medium containing either $^{15}NH_4Cl$ (1 g L^{-1}) or both [$^{13}C_6$]-D-glucose (2 g L^{-1}) and $^{15}NH_4Cl$ (1 g L^{-1}) from Cambridge Isotope Laboratories Inc., respectively. Except for the medium, other conditions were the same as for the unlabelled protein during growth and expression.

The cultured cells were harvested by centrifugation, and the pellets were resuspended in chilled buffer A (20 mM sodium phosphate pH 7.4, 274 mM NaCl, 5.4 mM KCl, 10% glycerol, 20 mM imidazole, 0.1 mg mL^{-1} lysozyme, 5 mM 2-mercaptoethanol, and cOmplete Protease Inhibitor Cocktail from Roche). The cells were then lysed by sonication and the cell debris was removed by centrifugation at 48000 *g* for 30 min. The supernatant was mixed with the Ni-NTA agarose beads (Qiagen) and shaken for 1 h at 4 °C. An affinity sorbent was separated from the unbound protein fraction by centrifugation at 3000 *g*, followed by decantation of the supernatant. The Ni-NTA agarose beads were washed three times with buffer A containing 30 mM imidazole. The WBSCR27 protein bound to the affinity sorbent was eluted with buffer A containing 350 mM imidazole. The fractions containing the WBSCR27 protein were collected, dialysed against buffer A, and cleaved with TEV protease (1% of WBSCR27 concentration) for 14 h at 4 °C. Untagged WBSCR27 was separated from TEV protease and cleaved 6His-S-tag using Ni-NTA agarose. The final protein contained residues 1–238 of WBSCR27 and two residues from the TEV cleavage site at the N-terminus.

The purified protein was concentrated to 0.2–0.6 mM and dialysed overnight against 1 L of buffer containing 50 mM sodium phosphate, 50 mM NaCl, 10 mM DTT, and 0.02% NaN_3, at pH 7.0 and 4 °C. All final protein solutions used were made using anoxic water by stirring it in vacuum for 20 min for degassing, to prevent DTT from oxidation.

Identification of the ligands co-purified with WBSCR27

After final dialysis, purified WBSCR27 (320 μL, 0.2 mM in 50 mM sodium phosphate, 50 mM NaCl, 10 mM dithiothreitol, and 0.02% NaN_3, at pH 7.0) was freeze-dried, re-dissolved in

D_2O, and denatured by DCl in D_2O (to pH of 1) to separate co-purified bound ligands. After 24 h at room temperature, the precipitated denatured protein was removed by centrifugation, and the ^1H NMR spectrum was measured. Comparison of the spectra to the ^1H NMR spectra of free SAM and SAH (Sigma Aldrich), measured in the same conditions, provided information about the resonance assignments. Integration of $H^{1'}$ resonances from both molecules gave a ratio of 1:2.7 between SAM and SAH.

Refolding of WBSCR27 to produce the apo form

The protein samples were dissolved in 8 mM urea and dialysed overnight against 1 L of 8 M urea to remove the SAM/SAH from the dialysis bag. Then the dialysis bag was moved to 250 mL refolding buffer (50 mM sodium phosphate, 50 mM NaCl, 3 mM DTT, and 0.02% NaN_3, at pH 7.0). The refolding buffer was changed four times over a period of 16 hours (the last time with 10 mM DTT). All dialysis procedures were performed at 4 °C.

NMR spectroscopy

The NMR samples, at a concentration of 0.5–0.6 mM for ^{13}C–^{15}N-labelled WBSCR27 and 0.1–0.6 mM for ^{15}N-labelled protein, were prepared in 95% H_2O/5% D_2O, 50 mM NaCl, 50 mM sodium phosphate buffer (pH 7.0), and 0.02% NaN_3. DTT at a concentration of 10 mM was added to the final solution to prevent oxidation of free cysteine residues. 3D triple-resonance (^1H, ^{13}C, ^{15}N) spectra were acquired at 35 °C on a Bruker AVANCE III 850 MHz spectrometer equipped with a z-gradient triple-resonance (^1H, ^{13}C, ^{15}N) probe (Academia Sinica, Taiwan). All other NMR experiments were conducted at 35 °C using a Bruker AVANCE 600 MHz spectrometer (Moscow State University). All 2D and 3D spectra were processed using NMRPipe software [65] and analysed using NMRFAM-Sparky [66]. 1D NMR spectra were processed and analysed using Mnova software (Mestrelab Research, Spain).

apo-WBSCR27 assignment

Backbone amide ^1H and ^{15}N resonance assignment of apo-WBSCR27 was performed using a triple-resonance sequential assignment scheme. For this purpose, the standard set of 3D experiments was measured: HNCO, HN(CA)CO, HN(CO)CA, HNCA, CBCA(CO)NH, HNCACB, HBHA(CO)NH, and HNHAHB, using ^{15}N-labelled or ^{13}C–^{15}N-labelled samples of apo-WBSCR27 at concentrations of 0.4 mM. Additionally, for side-chain assignment, data from ^{13}C HCCH-TOCSY were collected. In the case of a similar backbone amide signal position,

information on assignments for the WBSCR27–SAM complex [8] was used to facilitate spectrum analysis.

NMR titration experiments

Interaction of WBSCR27 with SAM, SAH, MTA, 5'dAdo, and adenine was studied using NMR titration experiments. ^{15}N-labelled apo-WBSCR27 samples at a concentration between 0.2 and 0.4 mM were used. The ligand concentration increased from 1 : 1 to 1 : 20 protein–ligand ratio. For each titration point, a ^{15}N–^{1}H SOFAST HMQC spectrum [67] was recorded. The resonances were assigned and the chemical shift perturbation data were calculated using the formula: $((\Delta\delta(^{1}H^{i}))^2 + (\Delta\delta(^{15}N^{i})/25)^2)^{½}$.

Values of K_d for MTA and 5'dAdo were estimated from NMR titration experiments carried out at 35 °C (Fig. S8). ^{1}H amide resonances of residues G79, V83, S101, and V166 were used in non-linear fitting of K_d values by the following equation [68]:

$$\Delta\delta_{obs} = \frac{\Delta\delta_{max}}{2[P]_0}\left[(K_d + [P]_0 + [L]_0) - \sqrt{(K_d + [P]_0 + [L]_0)^2 - 4[P]_0[L]_0}\,\right]$$

where P_0 and L_0 are the total concentrations of WBSCR27 and the ligand (MTA or 5'dAdo) in each titration step, $\Delta\delta_{obs}$ is the change of chemical shift value, and $\Delta\delta_{max}$ is the maximum change of the chemical shift accepted by the difference between the signal in free protein and protein in the presence of the maximum ligand concentration.

Isothermal titration calorimetry (ITC)

The thermodynamic parameters of WBSCR27 binding to SAM and SAH were measured using a MicroCal iTC200 instrument (GE Healthcare), as described elsewhere [69]. Experiments were carried out at 15, 25, and 37 °C in 50 mM phosphate buffer (pH 7.0) containing 50 mM NaCl, 10 mM DTT, and 0.2% sodium azide. Aliquots (2 μL) of SAM or SAH (200 μM) were injected into a 0.2 mL cell containing apo-WBSCR27 solution (20 μM) to achieve a complete binding isotherm. The heat of dilution was measured by injection of the ligand into the buffer solution or by additional injections of ligand after saturation; the values obtained were subtracted from the heat of reaction to obtain the effective heat of binding. The resulting titration curves were fitted using MicroCal Origin software, assuming one set of binding sites. Affinity constants (K_a) and enthalpy variations (ΔH) were determined, and the Gibbs energy (ΔG) and entropy variations (ΔS) were calculated from the equation: $-RT\ln K_a = \Delta G = \Delta H - T\Delta S$.

Tracing WBSCR27–SAH complex decomposition

To study bound SAH decomposition over time, a series of ^{15}N–^{1}H HSQC experiments were conducted using ^{15}N-labelled and ^{15}N–^{13}C-labelled WBSCR27 samples with a protein concentration of between 0.1 and 0.4 mM. Experiments were performed in Shigemi NMR tubes. Between measurements, samples were thermostatted at 35 °C with constant control of DTT concentration. The experiments lasted up to 17 days.

Tracing WBSCR27–SAM complex decomposition

To study bound SAM decomposition over time, a series of ^{15}N–^{1}H HSQC experiments were measured at 850 MHz using ^{15}N-labelled WBSCR27 samples with a protein concentration of 0.2 mM. Twelve HSQC experiments were collected during 4 hours, each 20 minutes long.

SAM decomposition in the presence and absence of WBSCR27

The impact of the WBSCR27 protein on SAM stability was assessed using 1D ^{1}H NMR. Samples contained SAM (1 mM) and WBSCR27 (67 μM) dissolved in D_2O in the presence of 50 mM sodium phosphate (pH 7.0), 50 mM NaCl, and 0.02% sodium azide. ^{1}H NMR spectra were collected immediately after sample preparation as well as after 122 h of thermostatting at 35 °C. Analogue samples were prepared with the same composition except WBSCR27, and treated with the same condition to be used as a control. DTT at a concentration of 5 mM was present in the sample which contained the protein.

Adenine cleavage from SAH, MTA, and 5'dAdo

Catalysis of adenine cleavage from SAH, MTA, and 5'dAdo by the WBSCR27 protein was monitored by ^{1}H NMR. The samples contained unlabelled WBSCR27 at a concentration of 30 μM, and one of the three ligands at a concentration of 0.3 mM. The samples also contained 50 mM sodium phosphate (pH 7.0), 50 mM NaCl, 0.02% sodium azide, and 10 mM DTT. All samples contained 5% D_2O. The amount of cleaved adenine was assessed using ^{1}H NMR (35 °C). Between measurements, samples were kept at 35 °C. DTT concentration in the samples was controlled by ^{1}H NMR. Analogue samples were prepared with the same composition except WBSCR27, and treated with the same conditions to be used as a control. The experiments were carried out for 144 hours with NMR spectra measured every 12 hours. The control experiment with SAH was carried out for 70 days with spectra measured in 3-4 days.

Acknowledgements

The Russian Foundation for Basic Research (grant 17-04-00852) supported the studies. Experiments on recombinant WBSCR27 production was supported by Russian Science Foundation (grant 19-14-00043). The 850 MHz NMR experiments were carried out using the equipment of the High-Field Nuclear Magnetic Resonance Center (HFNMRC) supported by Academia Sinica (AS-CFII-108-112), Taipei, Taiwan.

REFERENCES

1. Strømme, P., Bjømstad, P. G. & Ramstad, K. (2002) Prevalence Estimation of Williams Syndrome, *J Child Neurol.* **17**, 269-271.

2. Pober , B. R. (2010) Williams–Beuren Syndrome, *New Engl J Med.* **362**, 239-252.

3. Schubert, C. (2009) The genomic basis of the Williams – Beuren syndrome, *Cell Mol Life Sci.* **66**, 1178-1197.

4. Doll, A. & Grzeschik, K. H. (2001) Characterization of two novel genes, WBSCR20 and WBSCR22, deleted in Williams-Beuren syndrome, *Cytogenet Genome Res.* **95**, 20-27.

5. Merla, G., Ucla, C., Guipponi, M. & Reymond, A. (2002) Identification of additional transcripts in the Williams-Beuren syndrome critical region, *Hum Genet.* **110**, 429-438.

6. Haag, S., Kretschmer, J. & Bohnsack, M. T. (2015) WBSCR22/Merm1 is required for late nuclear pre-ribosomal RNA processing and mediates N7-methylation of G1639 in human 18S rRNA, *RNA.* **21**, 180-187.

7. Zorbas, C., Nicolas, E., Wacheul, L., Huvelle, E., Heurgué-Hamard, V. & Lafontaine, D. L. J. (2015) The human 18S rRNA base methyltransferases DIMT1L and WBSCR22-TRMT112 but not rRNA modification are required for ribosome biogenesis, *Mol Biol Cell.* **26**, 2080-2095.

8. Mariasina, S. S., Petrova, O. A., Osterman, I. A., Sergeeva, O. V., Efimov, S. V., Klochkov, V. V., Sergiev, P. V., Dontsova, O. A., Huang, T.-h., Chang, C.-F. & Polshakov, V. I. (2018) NMR assignments of the WBSCR27 protein related to Williams-Beuren syndrome, *Biomol NMR Assign.* **12**, 303-308.

9. Schubert, H. L., Blumenthal, R. M. & Cheng, X. (2003) Many paths to methyltransfer: a chronicle of convergence, *Trends Biochem Sci* **28**, 329-335.

10. Martin, J. L. & McMillan, F. M. (2002) SAM (dependent) I AM: the S-adenosylmethionine-dependent methyltransferase fold, *Cur Opin Struct Biol.* **12**, 783-793.

11. Fauman, E. B., Blumenthal, R. M. & Cheng, X. (1999) Structure and evolution of AdoMet-dependent methyltransferases in *S-adenosylmethionine-dependent methyltransferases: structures and functions* (Xiaodong, C., ed) pp. 1-38, World Scientific.

12. Gana, R., Rao, S., Huang, H., Wu, C. & Vasudevan, S. (2013) Structural and functional studies of S-adenosyl-L-methionine binding proteins: a ligand-centric approach, *BMC Struct Biol.* **13**, 6.

13. Liscombe, D. K., Louie, G. V. & Noel, J. P. (2012) Architectures, mechanisms and molecular evolution of natural product methyltransferases, *Nat Prod Rep.* **29**, 1238-1250.

14. Vertino, P. M. (1999) Eukaryotic DNA methyltransferases in *S-adenosylmethionine-dependent methyltransferases: structures and functions* (Xiaodong, C., ed) pp. 341-372, World Scientific.

15. Dryden, D. T. F. (1999) Bacterial DNA methyltranferases in *S-adenosylmethionine-dependent methyltransferases: structures and functions* (Xiaodong, C., ed) pp. 283-340, World Scientific.

16. Sergiev, P. V., Aleksashin, N. A., Chugunova, A. A., Polikanov, Y. S. & Dontsova, O. A. (2018) Structural and evolutionary insights into ribosomal RNA methylation, *Nat Chem Biol.* **14**, 226.

17. Motorin, Y. & Helm, M. (2011) RNA nucleotide methylation, *WIRES RNA.* **2**, 611-631.

18. Murn, J. & Shi, Y. (2017) The winding path of protein methylation research: milestones and new frontiers, *Nat Rev Mol Cell Biol.* **18**, 517.

19. Zhang, J. & Zheng, Y. G. (2016) SAM/SAH Analogs as Versatile Tools for SAM-Dependent Methyltransferases, *ACS Chem Biol.* **11**, 583-597.

20. Cantoni, G. L. (1975) Biological Methylation: Selected Aspects, *Ann Rev Biochem.* **44**, 435-451.

21. Hoffman, J. L. (1986) Chromatographic analysis of the chiral and covalent instability of S-adenosyl-L-methionine, *Biochemistry-US.* **25**, 4444-4449.

22. Giulidori, P., Galli-Kienle, M., Catto, E. & Stramentinoli, G. (1984) Transmethylation, transsulfuration, and aminopropylation reactions of S-adenosyl-L-methionine in vivo, *J Biol Chem.* **259**, 4205-4211.

23. Fontecave, M., Atta, M. & Mulliez, E. (2004) S-adenosylmethionine: nothing goes to waste, *Trends Biochem Sci.* **29**, 243-249.

24. Layer, G., Heinz, D. W., Jahn, D. & Schubert, W.-D. (2004) Structure and function of radical SAM enzymes, *Cur Opin Chem Biol.* **8**, 468-476.

25. Dong, M., Zhang, Y. & Lin, H. (2018) Noncanonical Radical SAM Enzyme Chemistry Learned from Diphthamide Biosynthesis, *Biochemistry.* **57**, 3454-3459.

26. Yang, H., Impano, S., Shepard, E. M., James, C. D., Broderick, W. E., Broderick, J. B. & Hoffman, B. M. (2019) Photoinduced Electron Transfer in a Radical SAM Enzyme Generates an S-Adenosylmethionine Derived Methyl Radical, *J Am Chem Soc.* **141**, 16117-16124.

27. Ueland, P. M. (1982) Pharmacological and biochemical aspects of S-adenosylhomocysteine and S-adenosylhomocysteine hydrolase, *Pharmacol Rev.* **34**, 223-253.

28. Walker, R. D. & Duerre, J. A. (1975) S-Adenosylhomocysteine Metabolism in Various Species, *Can J Biochem.* **53**, 312-319.

29. Parveen, N. & Cornell, K. A. (2011) Methylthioadenosine/S-adenosylhomocysteine nucleosidase, a critical enzyme for bacterial metabolism, *Mol Microbiol.* **79**, 7-20.

30. Shen, Y., Delaglio, F., Cornilescu, G. & Bax, A. (2009) TALOS plus : a hybrid method for predicting protein backbone torsion angles from NMR chemical shifts, *J Biomol NMR.* **44**, 213-223.

31. Jelesarov, I. & Bosshard, H. R. (1999) Isothermal titration calorimetry and differential scanning calorimetry as complementary tools to investigate the energetics of biomolecular recognition, *J Mol Recogn.* **12**, 3-18.

32. Connelly, P. R. & Thomson, J. A. (1992) Heat capacity changes and hydrophobic interactions in the binding of FK506 and rapamycin to the FK506 binding protein, *P Natl Acad Sci USA.* **89**, 4781-4785.

33. Fage, C. D., Isiorho, E. A., Liu, Y., Wagner, D. T., Liu, H.-w. & Keatinge-Clay, A. T. (2015) The structure of SpnF, a standalone enzyme that catalyzes [4 + 2] cycloaddition, *Nat Chem Biol.* **11**, 256-258.

34. Singh, S., McCoy, J. G., Zhang, C., Bingman, C. A., Phillips, G. N. & Thorson, J. S. (2008) Structure and Mechanism of the Rebeccamycin Sugar 4′-O-Methyltransferase RebM, *J Biol Chem.* **283**, 22628-22636.

35. Scheuermann, T. H., Lolis, E. & Hodsdon, M. E. (2003) Tertiary Structure of Thiopurine Methyltransferase from Pseudomonas syringae, a Bacterial Orthologue of a Polymorphic, Drug-metabolizing Enzyme, *J Mol Biol.* **333**, 573-585.

36. Pakhomova, S., Luka, Z., Grohmann, S., Wagner, C. & Newcomer, M. E. (2004) Glycine N-methyltransferases: A comparison of the crystal structures and kinetic properties of recombinant human, mouse and rat enzymes, *Proteins.* **57**, 331-337.

37. Bheemanaik, S., Reddy, Yeturu V. R. & Rao, Desirazu N. (2006) Structure, function and mechanism of exocyclic DNA methyltransferases, *Biochem J.* **399**, 177-190.

38. Lesnyak, D. V., Osipiuk, J., Skarina, T., Sergiev, P. V., Bogdanov, A. A., Edwards, A., Savchenko, A., Joachimiak, A. & Dontsova, O. A. (2007) Methyltransferase That Modifies Guanine 966 of the 16 S rRNA: functional identification and tertiary structure, *J Biol Chem.* **282**, 5880-5887.

39. Kumar, A., Saigal, K., Malhotra, K., Sinha, K. M. & Taneja, B. (2011) Structural and Functional Characterization of Rv2966c Protein Reveals an RsmD-like Methyltransferase from Mycobacterium tuberculosis and the Role of Its N-terminal Domain in Target Recognition, *J Biol Chem.* **286**, 19652-19661.

40. Sergiev, P. V., Serebryakova, M. V., Bogdanov, A. A. & Dontsova, O. A. (2008) The ybiN Gene of Escherichia coli Encodes Adenine-N6 Methyltransferase Specific for Modification of A1618 of 23 S Ribosomal RNA, a Methylated Residue Located Close to the Ribosomal Exit Tunnel, *J Mol Biol.* **375**, 291-300.

41. Ruszkowska, A., Ruszkowski, M., Dauter, Z. & Brown, J. A. (2018) Structural insights into the RNA methyltransferase domain of METTL16, *Sci Rep.* **8**, 5311.

42. Foster, P. G., Nunes, C. R., Greene, P., Moustakas, D. & Stroud, R. M. (2003) The First Structure of an RNA m5C Methyltransferase, Fmu, Provides Insight into Catalytic Mechanism and Specific Binding of RNA Substrate, *Structure.* **11**, 1609-1620.

43. Sunita, S., Purta, E., Durawa, M., Tkaczuk, K. L., Swaathi, J., Bujnicki, J. M. & Sivaraman, J. (2007) Functional specialization of domains tandemly duplicated within 16S rRNA methyltransferase RsmC, *Nucl Acids Res.* **35**, 4264-4274.

44. Dégut, C., Roovers, M., Barraud, P., Brachet, F., Feller, A., Larue, V., Al Refaii, A., Caillet, J., Droogmans, L. & Tisné, C. (2019) Structural characterization of *B. subtilis* m1A22 tRNA methyltransferase TrmK: insights into tRNA recognition, *Nucl Acids Res.* **47**, 4736-4750.

45. Hallberg, B. M., Ericsson, U. B., Johnson, K. A., Andersen, N. M., Douthwaite, S., Nordlund, P., Beuscher, A. E. & Erlandsen, H. (2006) The Structure of the RNA m5C Methyltransferase YebU from Escherichia coli Reveals a C-terminal RNA-recruiting PUA Domain, *J Mol Biol.* **360**, 774-787.

46. Bussiere, D. E., Muchmore, S. W., Dealwis, C. G., Schluckebier, G., Nienaber, V. L., Edalji, R. P., Walter, K. A., Ladror, U. S., Holzman, T. F. & Abad-Zapatero, C. (1998) Crystal Structure of ErmC‘, an rRNA Methyltransferase Which Mediates Antibiotic Resistance in Bacteria, *Biochemistry-US.* **37**, 7103-7112.

47. Jeltsch, A. (2002) Beyond Watson and Crick: DNA Methylation and Molecular Enzymology of DNA Methyltransferases, *ChemBioChem.* **3**, 274-293.

48. Brecher, M. B., Li, Z., Zhang, J., Chen, H., Lin, Q., Liu, B. & Li, H. (2015) Refolding of a fully functional flavivirus methyltransferase revealed that S-adenosyl methionine but not S-adenosyl homocysteine is copurified with flavivirus methyltransferase, *Protein Sci.* **24**, 117-128.

49. Lim, S. P., Sonntag, L. S., Noble, C., Nilar, S. H., Ng, R. H., Zou, G., Monaghan, P., Chung, K. Y., Dong, H., Liu, B., Bodenreider, C., Lee, G., Ding, M., Chan, W. L., Wang, G., Jian, Y. L., Chao, A. T., Lescar, J., Yin, Z., Vedananda, T. R., Keller, T. H. & Shi, P.-Y. (2011) Small Molecule Inhibitors That Selectively Block Dengue Virus Methyltransferase, *J Biol Chem.* **286**, 6233-6240.

50. Miller, D. J., Ouellette, N., Evdokimova, E., Savchenko, A., Edwards, A. & Anderson, W. F. (2003) Crystal complexes of a predicted S-adenosylmethionine-dependent methyltransferase reveal a typical AdoMet binding domain and a substrate recognition domain, *Protein Sci.* **12**, 1432-1442.

51. Griffith, S. C., Sawaya, M. R., Boutz, D. R., Thapar, N., Katz, J. E., Clarke, S. & Yeates, T. O. (2001) Crystal structure of a protein repair methyltransferase from Pyrococcus furiosus with its l-isoaspartyl peptide substrate11Edited by I. A. Wilson, *J Mol Biol.* **313**, 1103-1116.

52. Liu, S., Wolfe, M. S. & Borchardt, R. T. (1992) Rational approaches to the design of antiviral agents based on S-adenosyl-l-homocysteine hydrolase as a molecular target, *Antivir Res.* **19**, 247-265.

53. Sergeeva, O. V., Prokhorova, I. V., Ordabaev, Y., Tsvetkov, P. O., Sergiev, P. V., Bogdanov, A. A., Makarov, A. A. & Dontsova, O. A. (2012) Properties of small rRNA methyltransferase RsmD: Mutational and kinetic study, *RNA.* **18**, 1178-1185.

54. Tongsook, C., Uhl, M. K., Jankowitsch, F., Mack, M., Gruber, K. & Macheroux, P. (2016) Structural and kinetic studies on RosA, the enzyme catalysing the methylation of 8-demethyl-8-amino-d-riboflavin to the antibiotic roseoflavin, *FEBS J.* **283**, 1531-1549.

55. Halliday, N. M., Hardie, K. R., Williams, P., Winzer, K. & Barrett, D. A. (2010) Quantitative liquid chromatography–tandem mass spectrometry profiling of activated methyl cycle metabolites involved in LuxS-dependent quorum sensing in *Escherichia coli*, *Anal Biochem.* **403**, 20-29.

56. Hoffman, D. R., Cornatzer, W. E. & Duerre, J. A. (1979) Relationship between tissue levels of S-adenosylmethionine, S-adenosylhomocysteine, and transmethylation reactions, *Can J Biochem.* **57**, 56-64.

57. Siegrist, J., Netzer, J., Mordhorst, S., Karst, L., Gerhardt, S., Einsle, O., Richter, M. & Andexer, J. N. (2017) Functional and structural characterisation of a bacterial O-methyltransferase and factors determining regioselectivity, *FEBS Lett.* **591**, 312-321.

58. Cornell, K. A., Swarts, W. E., Barry, R. D. & Riscoe, M. K. (1996) Characterization of RecombinantEschericha coli5′-Methylthioadenosine/S-Adenosylhomocysteine Nucleosidase: Analysis of Enzymatic Activity and Substrate Specificity, *Biochem Bioph Res Commun.* **228**, 724-732.

59. de la Haba, G. & Cantoni, G. L. (1959) The Enzymatic Synthesis of S-Adenosyl-l-homocysteine from Adenosine and Homocysteine, *J Biol Chem.* **234**, 603-608.

60. Lee, J. E., Cornell, K. A., Riscoe, M. K. & Howell, P. L. (2001) Structure of E. coli 5′-methylthioadenosine/S-adenosylhomocysteine Nucleosidase Reveals Similarity to the Purine Nucleoside Phosphorylases, *Structure.* **9**, 941-953.

61. Tsuji, E., Okazaki, K., Isaji, M. & Takeda, K. (2009) Crystal structures of the Apo and Holo form of rat catechol-O-methyltransferase, *J Struct Biol.* **165**, 133-139.

62. Pattanayek, R., Newcomer, M. E. & Wagner, C. (1998) Crystal structure of apo-glycine N-methyltransferase (GNMT), *Protein Sci.* **7**, 1326-1331.

63. Kim, J. & Almo, S. C. (2013) Structural basis for hypermodification of the wobble uridine in tRNA by bifunctional enzyme MnmC, *BMC Struct Biol.* **13**, 5.

64. Jiang, Y., Li, J., Ren, F., Ji, C., Aniagu, S. & Chen, T. (2019) PM2.5-induced extensive DNA methylation changes in the heart of zebrafish embryos and the protective effect of folic acid, *Environ Pollut.* **255**, 113331.

65. Delaglio, F., Grzesiek, S., Vuister, G. W., Zhu, G., Pfeifer, J. & Bax, A. (1995) NMRPipe: a multidimensional spectral processing system based on UNIX pipes, *J Biomol NMR.* **6**, 277-93.

66. Lee, W., Tonelli, M. & Markley, J. L. (2015) NMRFAM-SPARKY: enhanced software for biomolecular NMR spectroscopy, *Bioinformatics.* **31**, 1325-1327.

67. Schanda, P., Kupče, Ē. & Brutscher, B. (2005) SOFAST-HMQC Experiments for Recording Two-dimensional Deteronuclear Correlation Spectra of Proteins within a Few Seconds, *J Biomol NMR.* **33**, 199-211.

68. Polshakov, V. I., Batuev, E. A. & Mantsyzov, A. B. (2019) NMR screening and studies of target–ligand interactions, *Russ Chem Rev.* **88**, 59-98.

69. Petrushanko, I. Y., Mitkevich, V. A., Anashkina, A. A., Klimanova, E. A., Dergousova, E. A., Lopina, O. D. & Makarov, A. A. (2014) Critical role of γ-phosphate in structural transition of Na,K-ATPase upon ATP binding, *Sci Rep.* **4**, 5165.

Table 1. Thermodynamic parameters of WBSCR27 binding to SAM and SAH determined by isothermal titration calorimetry[a].

Ligand	T, °C	K_a[b], M^{-1}	K_d[c], μM	ΔH[d], kcal mol^{-1}	TΔS[e], kcal mol^{-1}	ΔG[f], kcal mol^{-1}
SAM	15	2.3×10^6	0.4	−19.3	−10.9	−8.4
SAM	25	8.5×10^5	1.2	−24.9	−16.8	−8.1
SAM	37	3.4×10^5	2.9	−31.0	−23.2	−7.8
SAH	15	11.9×10^6	0.08	−22.5	−13.0	−9.5
SAH	25	4.5×10^6	0.22	−28.9	−19.8	−9.1
SAH	37	6.2×10^5	1.61	−37.0	−28.8	−8.2

[a] All measurements were performed two to four times in a 50 mM phosphate buffer (pH 7.0) containing 50 mM NaCl, 10 mM DTT, and 0.2% sodium azide.

[b] K_a – affinity constant; standard deviation did not exceed ± 20%.

[c] K_d – dissociation constant; calculated as $1/K_a$.

[d] ΔH – enthalpy variation; standard deviation did not exceed ± 10%.

[e] TΔS – entropy variation; calculated from the equation $\Delta G = \Delta H - T\Delta S$.

[f] ΔG – Gibbs energy; calculated from the equation $\Delta G = -RTlnK_a$.

Table 2. Heat capacity changes and solvent-accessible surface area for WBSCR27 binding to SAM and SAH[a].

Ligand	ΔC_p (cal mol^{-1} K^{-1})	SAA_{min}[b] (Å^2)	SAA_{max}[b] (Å^2)
SAM	−530	1325	1963
SAH	−660	1650	2444

[a] Heat capacity changes were obtained as d(ΔH)/dT.

[b] Changes in SAA were estimated using the following formula: $\Delta C_p = 0.27\Delta A_{aromatic} + 0.4\Delta A_{non\text{-}aromatic}$, where $\Delta A_{aromatic}$ and $\Delta A_{non\text{-}aromatic}$ are the protected areas due to aromatic and non-aromatic amino acids in Å^2, respectively [32]. SAA_{min} and SAA_{max} are calculated assuming that all the changes are conferred by non-aromatic and aromatic residues, respectively.

FIGURES

Scheme 1. Main pathways of SAM usage *in vivo*. Path 1 represents removal of the methyl group in a methyltransferase-catalysed methylation reaction. Path 2 is a non-enzymatic transformation of SAM to MTA and homoserine lactone. Paths 3 and 4 represent an enzyme-catalysed cleavage of the bonds between the sulfur and neighbour carbons with the formation of the reactive 5'-deoxyadenosyl and ACP radicals.

Scheme 2. Adenine cleavage reactions catalysed by WBSCR27. The nucleosidase activity of the methyltransferase WBSCR27 causes the adenine cleavage from SAH, MTA, and 5'dAdo.

Figure 1. Identification of the ratio of ligands bound to WBSCR27. (**A**) ^{1}H signals of the co-purified ligands after protein denaturation and precipitation; (**B**) ^{1}H signals of free SAH; (**C**) ^{1}H signals of free SAM. Integral intensity of peaks corresponds to a ratio of 1.0:2.7 between WBSCR27–SAM and WBSCR27–SAH complexes.

Figure 2. ^{15}N–^{1}H HSQC spectrum of *Mus musculus* WBSCR27 in apo form. The spectrum was recorded at a proton resonance frequency of 850 MHz, 35°C in 50 mM sodium phosphate, pH 7.0, 50 mM NaCl, 5 mM DTT and 0.2% NaN_3. Protein concentration is 0.4 mM.

Figure 3. Results for prediction of the secondary structure by TALOS+ [30] based on NMR chemical shift assignments for (A) apo-WBSCR27 (red) and (B) complex of WBSCR27 with SAH (blue). Values of chemical shift indices (CSI) are shown as vertical bars (positive for α-helices and negative for β-strands). Absolute values of bars are equal to the probability of the existence of a corresponding amino acid residue in one or another element of the secondary structure.

Figure 4. Transformation of the complex WBSCR27-SAH to the apo form. In the centre is the overlay of the ^{15}N-^{1}H HSQC spectra of WBSCR27-SAH (blue) and apo-WBSCR27 (red). The perimeter panels show selected fragments of spectra measured at certain time intervals at 35°C. The disappearance of the characteristic signals of the complex and the appearance of the signals of apo form indicates that the complex slowly undergoes transformation to the apo-WBSCR27.

Figure 5. Transformation of the complex of WBSCR27 with SAM to the complex WBSCR27-SAH. A. Overlay of the ^{15}N-^{1}H HSQC spectra for the complex WBSCR27-SAM (red) and

WBSCR27-SAM (black). B-E. Representative fragment of the ^{15}N-^{1}H HSQC spectra of WBSCR27-SAM recorded immediately after addition of equimolar amount of SAM to the protein (B) and after 1, 3 and 20 hours at 35 °C (C, D and E correspondingly. indicating that SAM bound to WBSCR27 undergoes transformation to SAH. Appearance of the signals of WBSCR27–SAH complex indicates demethylation of SAM.

Figure 6. Fragments of 1D ^{1}H NMR spectra, illustrating the decomposition of SAM at 35 °C in the free state (A, B) and in the presence of catalytic quantities of WBSCR27 (C, D). Spectra A and C were recorded immediately after preparation of the samples; spectra B and D were collected after 122 h at 35 °C. The concentration of SAM was 1 mM in D_2O. All solutions contained 50 mM sodium phosphate (pH 7.0) and 50 mM NaCl. The concentration of WBSCR27 (C, D) was 67 μM. Solutions containing WBSCR27 also contained DTT at a concentration of 5 mM.

Figure 7. Adenine cleavage by WBSCR27 from SAH, MTA, and 5'dAdo. Reaction mixtures contained 0.3 mM SAH (**A**), MTA (**B**), or 5'dAdo (**C**), respectively, with 30 μM WBSCR27 in buffer containing 50 mM NaCl, 50 mM sodium phosphate at pH 7.0, 0.02% sodium azide, and 10 mM DTT at 35 °C. Total incubation time was 144 h.

Figure 8. Histograms of ^{1}H and ^{15}N chemical shift perturbations for the protein backbone amide groups between apo-WBSCR27 and corresponding complexes: (A) WBSCR27–SAH, (B) WBSCR27–SAM, (C) WBSCR27–MTA, (D) WBSCR27–5'dAdo, and (E) WBSCR27–adenine. Chemical shift perturbations for each *i*-th residue were calculated using the following equation: $CSP^{i} = ((\Delta\delta(^{1}H^{i}))^2 + (\Delta\delta(^{15}N^{i})/25)^2)^{½}$.

Figure 9. Structure of several Class I MTases. **A**, SAM-dependent methyltransferase SpnF, involved in the biosynthesis of spinosyn insecticides (PDB ID 4PNE); **B**, ubiquinone/menaquinone biosynthesis methyltransferase from *Thermotoga maritima* (PDB ID 2AVN); **C**, methyltransferase from *Bacillus thuringiensis* (PDB ID 3L8D); **D**, rebeccamycin 4'-O-methyltransferase RebM (PDB ID 3BUS); **E**, *Saccharomyces cerevisiae* methyltransferase Bud23 (PDB ID 4QTU); **F**, human glycine N-methyltransferase (PDB ID 1R74). Structures were drawn using the Discovery Studio Visualizer v. 16 from Dassault Systemes Biovia Co.

Figure 10. Schematic drawing of WBSCR27 in the complex with SAH or SAM. Labels indicate the elements of the secondary structure and the number of amino acid residues located at the

boundaries of α-helices or β-strands. Residues with large chemical shift perturbations upon binding of SAH (> 0.1) are coloured magenta. Elements of the secondary structure were drawn using the Discovery Studio Visualizer v. 16 from Dassault Systemes Biovia Co.

SUPPORTING INFORMATION

Figure S1. ^{1}H NMR spectra of SAH, indicating that free SAH (without the presence of WBSCR27) remains stable for more than 70 days at room temperature.

Figure S2. Isothermal titration calorimetry of apo-WBSCR27 with SAM and SAH at different temperatures. A buffered solution of SAM or SAH (concentration of the cofactors 200 μM) was titrated into a solution of WBSCR27 (7 μM) containing the same buffer. The resulting isotherm data were fitted to a single-site model.

Figure S3. Overlay of the ^{1}H-^{15}N HSQC spectra of ^{15}N-labelled apo-WBSCR27 (0.18 mM) titrated by an increasing amount of 5'dAdo.

Figure S4. Overlay of the ^{1}H-^{15}N HSQC spectra of ^{15}N-labelled apo-WBSCR27 (0.18 mM) titrated by an increasing amount of MTA.

Figure S5. Overlay of the ^{1}H-^{15}N HSQC spectra of 0.4 mM ^{15}N-labelled WBSCR27 in the apo state (red), in the presence of 5 mM SAH (blue), and 7.6 mM adenine (cyan).

Figure S6. Representative fragments of overlaid ^{15}N-^{1}H HSQC spectra of WBSCR27 recorded for free protein (black) and in the presence of a 10-fold molar excess of SAH (red), 20-fold molar excess of MTA (cyan), 20-fold molar excess of 5'dAdo (blue), and 19-fold molar excess of adenine (orange). Fragments of spectra containing backbone amide resonances G123 (A), G79, V83, L127, S101 (B), T121, V140, C167 (C), V76, and D99 (D) are illustrated.

Figure S7. Multiple sequence alignment of WBSCR27 protein and its closest analogues with known 3D structure. Sequences were selected from Universal Protein Resource (UniProt) and aligned using the CLUSTAL Omega (v. 1.2.4) software.

Figure S8. Fragments of the overlaid ^{1}H-^{15}N HSQC spectra of ^{15}N-labelled apo-WBSCR27 (0.18 mM) with an increasing amount of MTA (A) and 5'dAdo (B) used in calculation of the K_d values for the ligands. Values of K_d estimated at 35 °C by non-linear fitting of the ^{1}H chemical shifts for MTA = 40 ± 10 μM, and for 5'dAdo = 100 ± 60 μM.

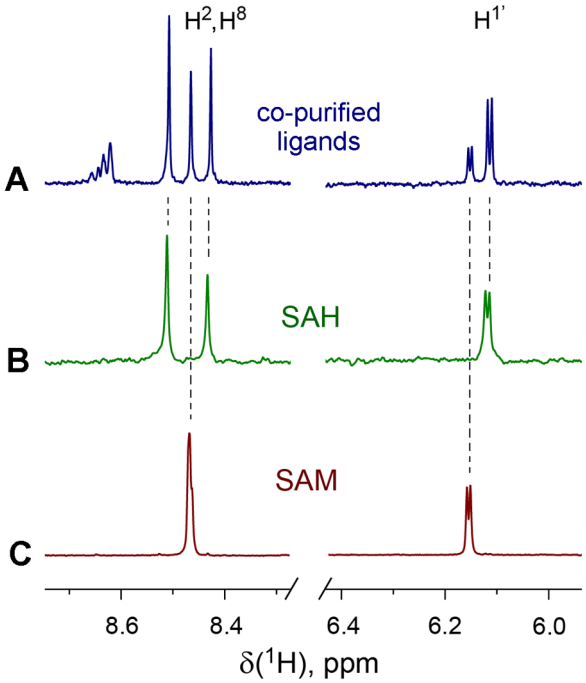

febs_15320_f1.tif

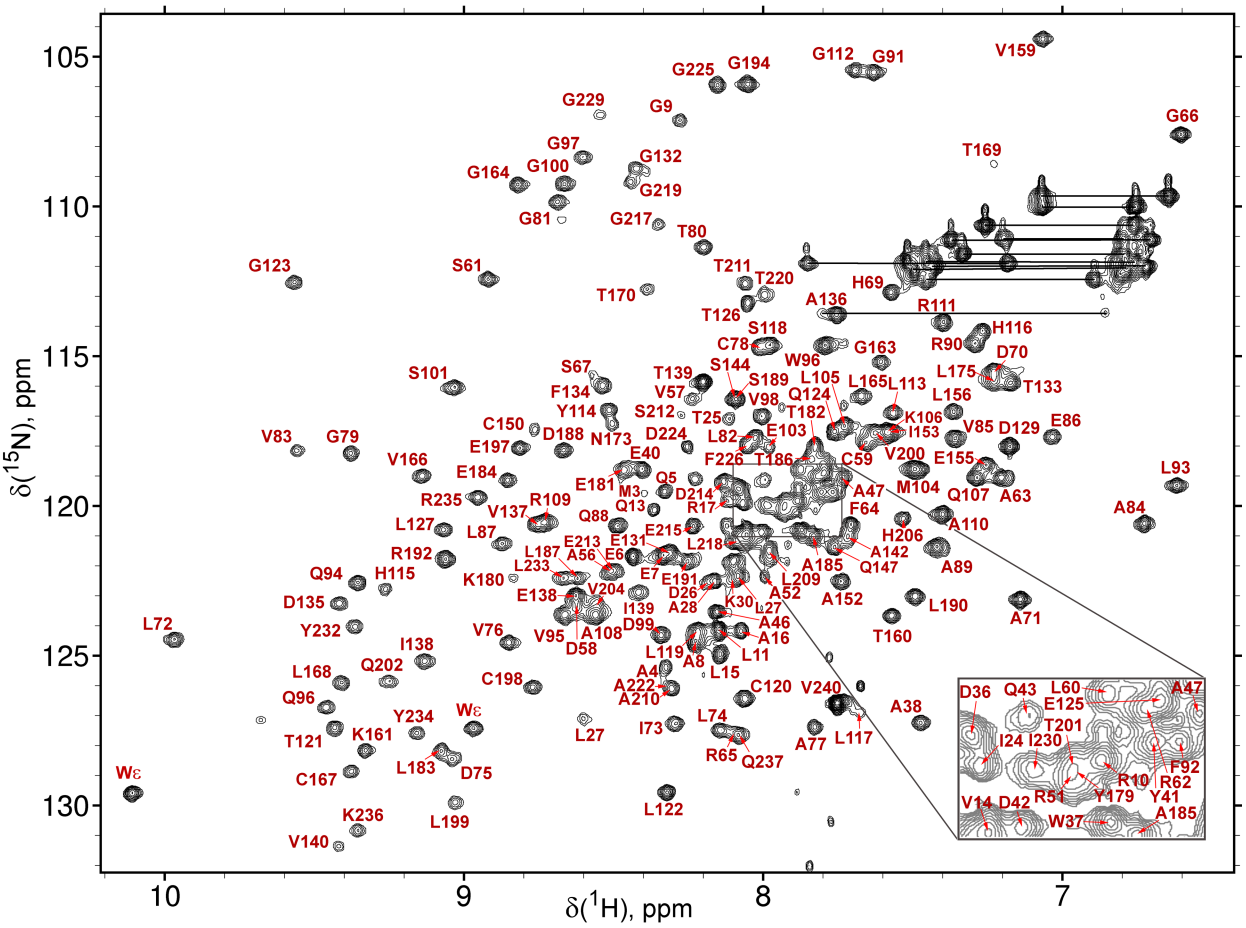

febs_15320_f2.tif

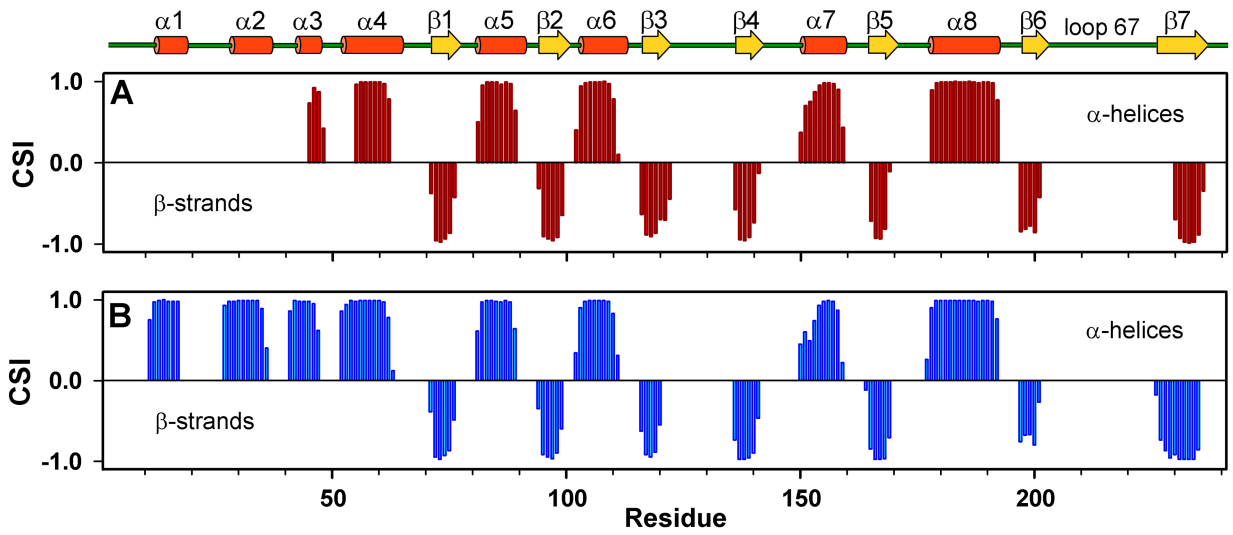

febs_15320_f3.tif

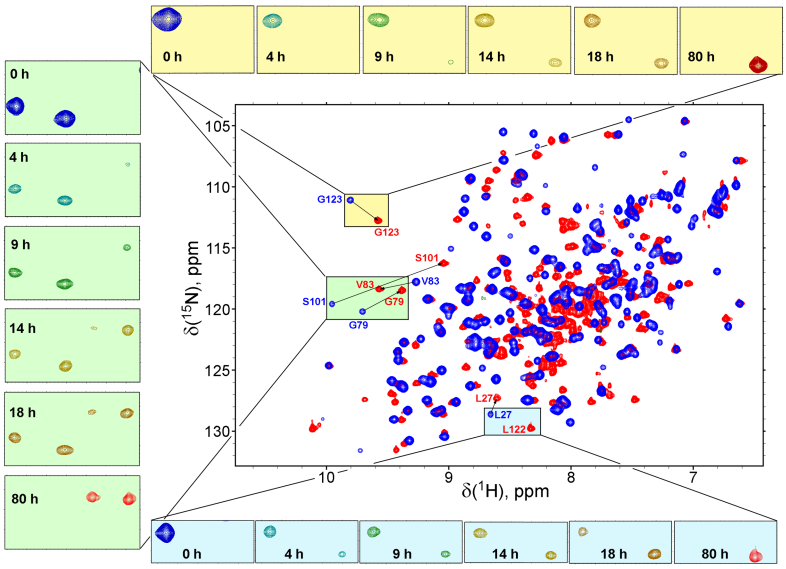

febs_15320_f4.tif

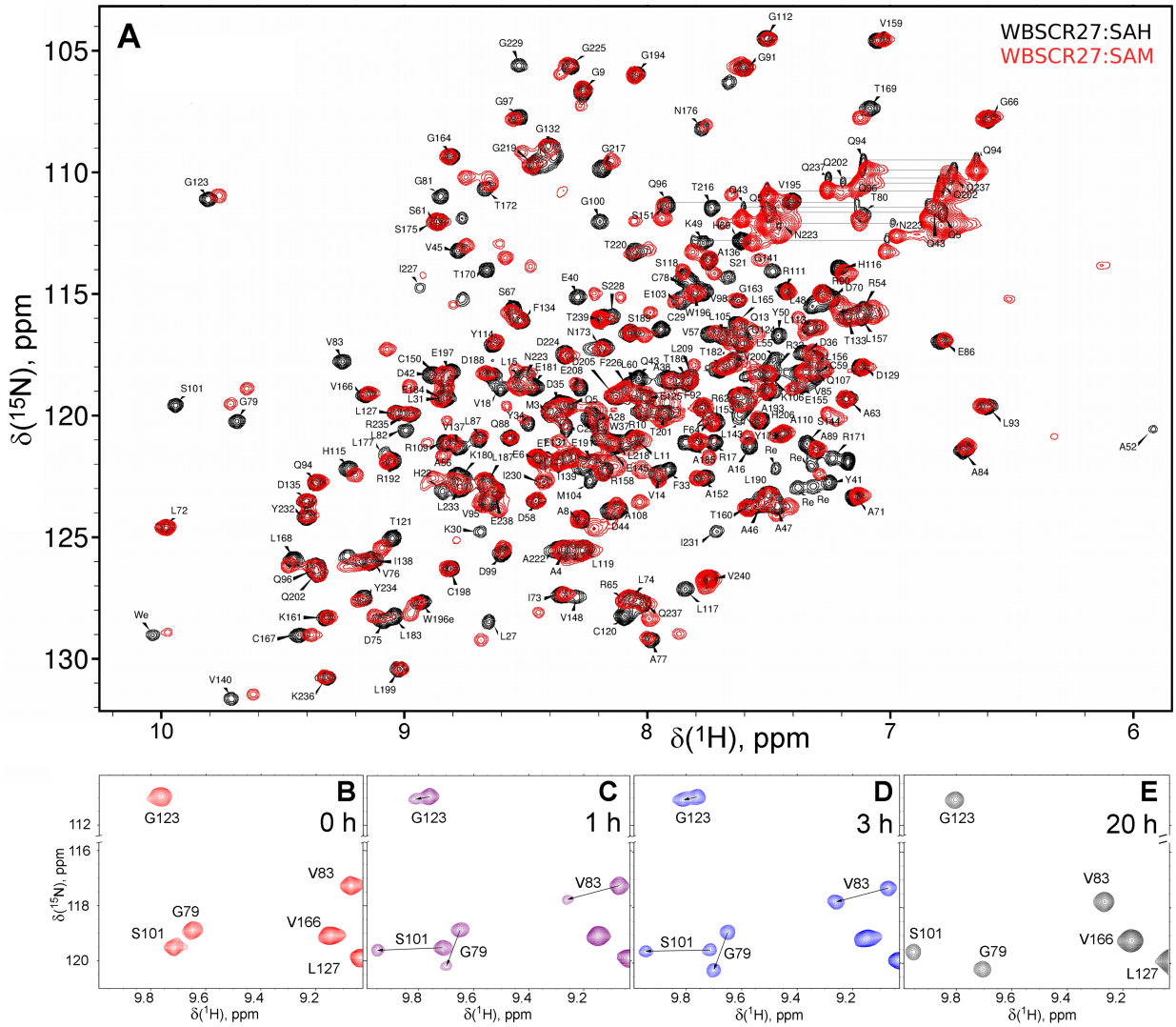

febs_15320_f5.tif

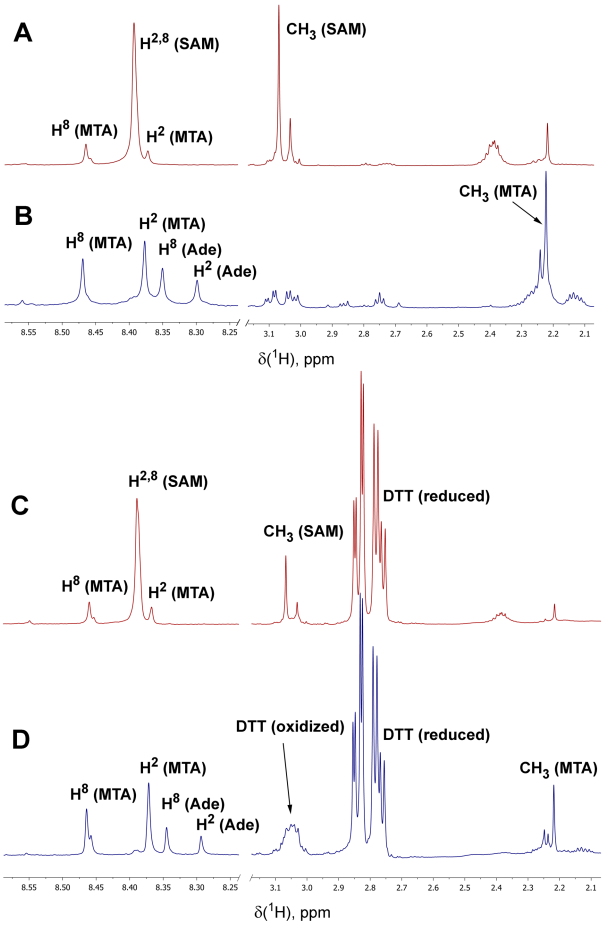

febs_15320_f6.tif

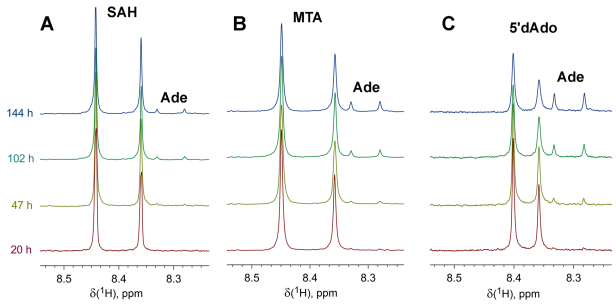

febs_15320_f7.tif

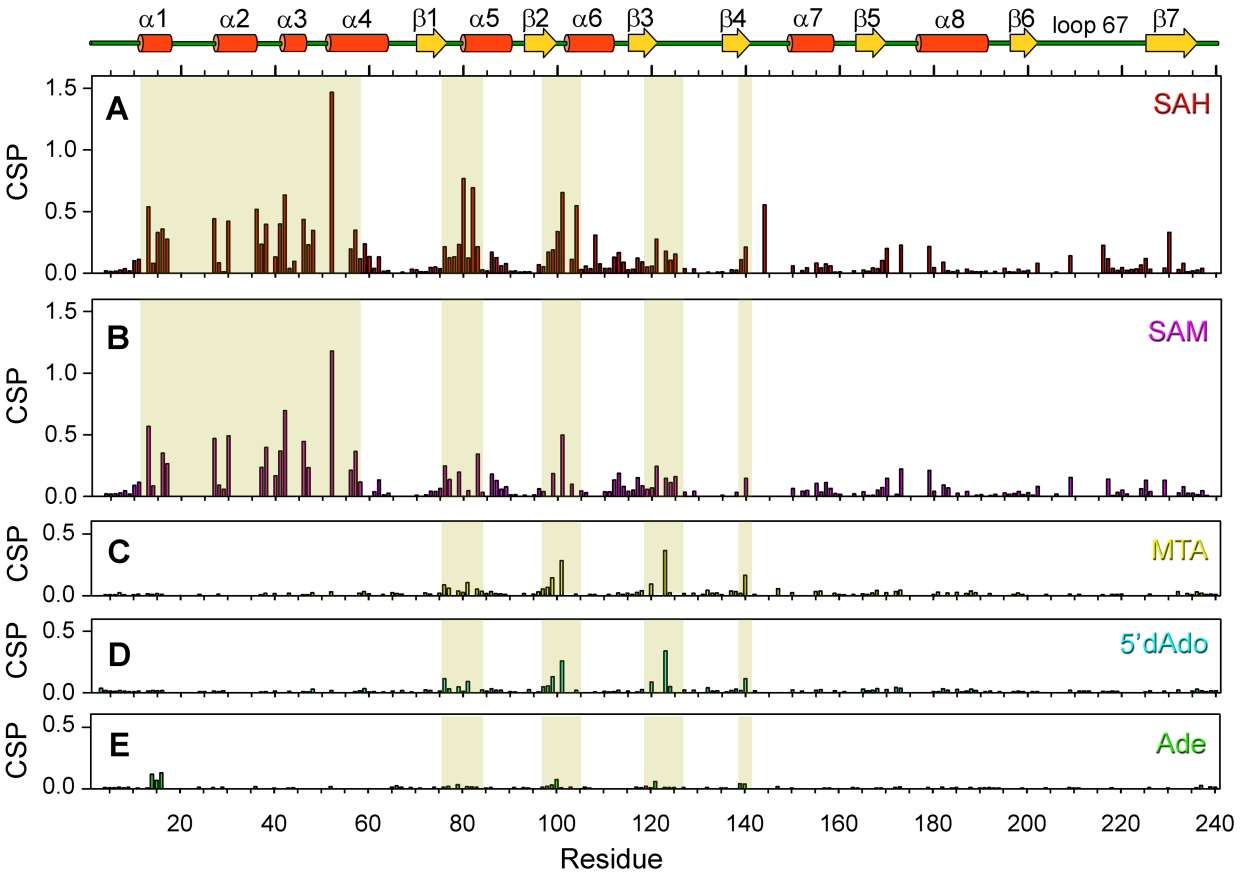

febs_15320_f8.tif

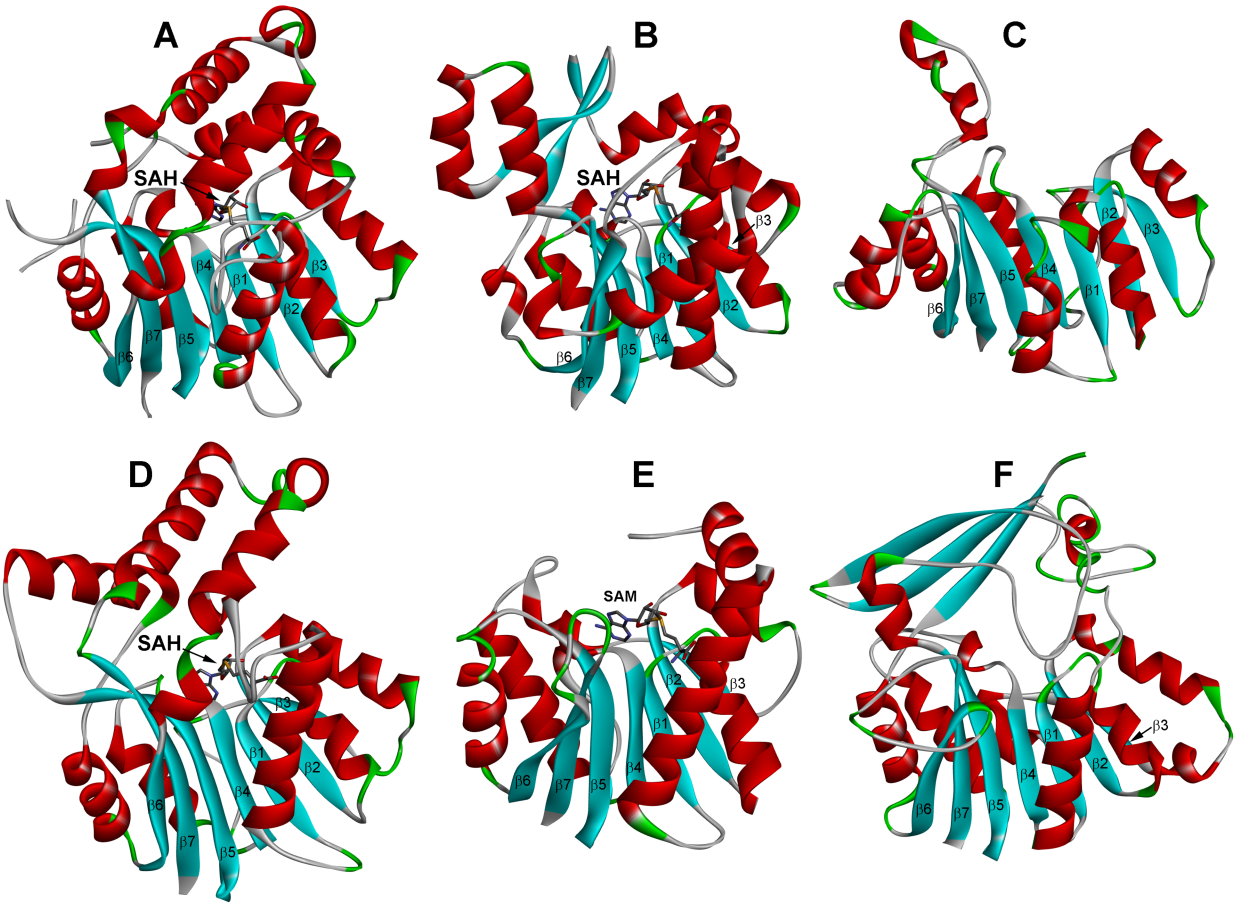

febs_15320_f9.tif

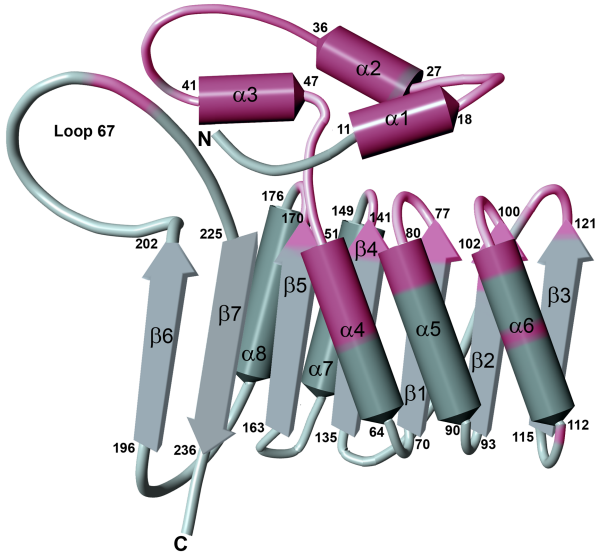

febs_15320_f10.tif

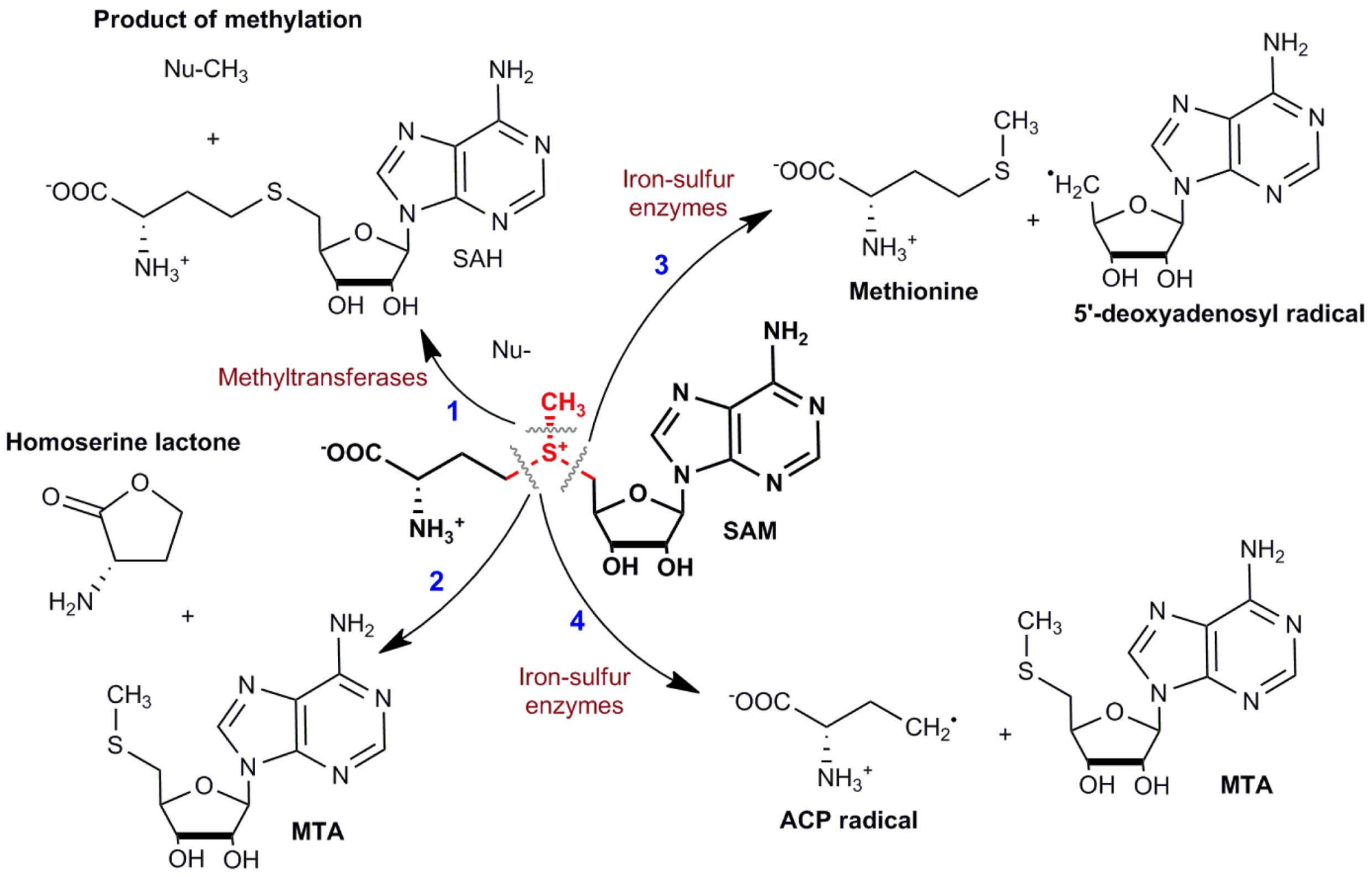
Product of methylation
Nu-CH3
+
-OOC
NH3+
S
O
OH OH
N
NH2
SAH
Methyltransferases
Nu-
1
Homoserine lactone
O
H2N
+
2
MTA
Iron-sulfur enzymes
3
Methionine
5'-deoxyadenosyl radical
CH3
S+
-OOC
NH3+
SAM
4
Iron-sulfur enzymes
ACP radical
CH2•
MTA

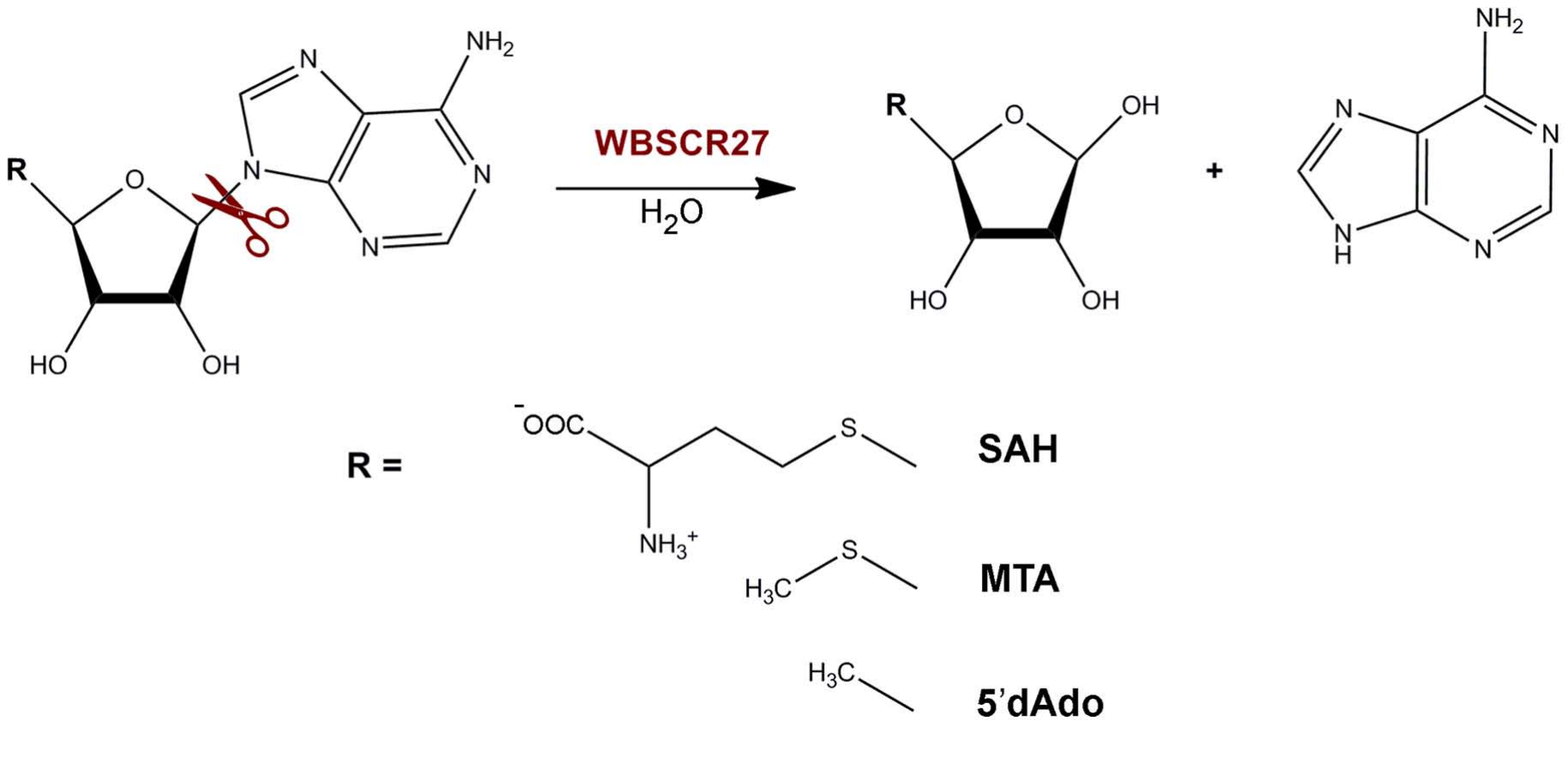
WBSCR27
H2O
R =
SAH
MTA
5'dAdo